Available online at www.sciencedirect.com

ScienceDirect

Journal of Magnesium and Alloys 7 (2019) 584–596

www.elsevier.com/locate/jma

Full Length Article

Bioactivity enhancement by Sr doped Zn-Ca-P coatings on biomedical magnesium alloy

P. Amaravathy, T.S. Sampath Kumar*

Medical Materials Laboratory, Department of Metallurgical and Materials Engineering, Indian Institute of Technology Madras, Chennai 600 036, India

Received 28 June 2018; received in revised form 27 May 2019; accepted 27 May 2019
Available online 18 November 2019

Abstract

The effect of strontium doped Zn-Ca-P (ZCP) coating by chemical conversion technique on the biodegradation of AZ31 alloy was evaluated. The coating formed with 1.5 wt.% Sr and 20 min phosphating time at 50 °C with pH 2.5 completely covers the alloy surface. The Sr doped coated sample also showed very low evolved hydrogen gas and pH change than the ZCP coatings suggested that the degradation of the alloy was extremely controlled. The *in vitro* bioactivity studies in simulated body fluid exhibits deposition of calcium phosphate phases with Ca/P ratio of 1.55 which is close to that of hydroxyapatite, mineral component of bone. Cytotoxicity evaluation with L929 cells showed higher cell viability of the Sr doped coatings compared to ZCP coatings.
© 2019 Published by Elsevier B.V. on behalf of Chongqing University.
This is an open access article under the CC BY-NC-ND license. (http://creativecommons.org/licenses/by-nc-nd/4.0/)
Peer review under responsibility of Chongqing University

Keywords: Magnesium alloy; Zinc calcium phosphate; Biocompatibility; Corrosion; Strontium; Cell viability.

1. Introduction

Magnesium alloys have been evolving as a promising biodegradable material due to its favourable mechanical properties and biocompatibility [1,2]. Moreover, magnesium is an important element found in human body and is involved in body metabolic activities such as protein synthesis, muscle contraction and relaxation, energy transport etc. [3]. Low levels of magnesium in human body lead to neurological, muscular and attention deficit hyperactivity disorders (ADHD) [4]. At present, magnesium alloys are used for biodegradable orthopedic implant applications such as screws, pins and stents. Although magnesium has many favourable properties due to its higher standard (negative) electrode potential value (−2.37 V vs. Standard Hydrogen Electrode (SHE)), it has the tendency to dissolve and thereby resulting in rapid corrosion, increase in local pH, hydrogen evolution, loss of their mechanical integrity before bone healing process [5,6]. However, the requirement of any biodegradable implants is that the degradation rate should be matched with the healing rate of bone [7]. Typically, magnesium alloys should maintain its mechanical integrity at least for 3 months for new bone formation [8].

Mainly three approaches have been developed to control the degradation rate of magnesium such as alloying, surface modification and coating [9]. Coating is one of the key solutions to overcome the corrosion rate of magnesium alloy in chloride containing environment by providing some barrier effects between the material and the environment. Various surface treatment techniques such as physical vapor deposition, electrodeposition, anodization, chemical vapour deposition, microarc oxidation were attempted to achieve desired coating [10]. Protective coatings with various functionalized polymeric groups such as polylactic acid (PLA), poly (latic-co-glycolic) acid (PLGA), polycaprolactone (PCL), polydopamine (PDA), chitosan (CS), collagen (Col) were attempted to control the degradation and improve the biocompatibility of magnesium alloys [11]. But long process time, high cost, high temperature and complex procedures seem to limit wide spread use of these techniques. In contrast, chemical conversion coating process is very simple, economic and

* Corresponding author.
E-mail address: tssk@iitm.ac.in (T.S.S. Kumar).

https://doi.org/10.1016/j.jma.2019.05.014
2213-9567/© 2019 Published by Elsevier B.V. on behalf of Chongqing University. This is an open access article under the CC BY-NC-ND license. (http://creativecommons.org/licenses/by-nc-nd/4.0/) Peer review under responsibility of Chongqing University

without the requirement of any instruments for the coating process. [12] As the coating is formed through the chemical reaction of metal with the electrolyte, it becomes the integral part of the alloy surface which may be essential for the highly degradable magnesium alloys [13].

Recently zinc phosphate, calcium phosphate and zinc calcium phosphate (ZCP) coatings have become attractive for magnesium alloys, as they can produce corrosion resistant coatings with high adhesion strength [14–21]. Zeng et al. studied the effect of solution temperature on the corrosion resistance of Mg-Li-Ca alloy [22] Doping is one of the effective strategy to improve bioactivity of the coatings and bioactive dopant ions such as Mg^{2+}, Cu^{2+}, Mn^{2+}, Sr^{2+} and Zn^{2+} have many physiological roles including bone formation process [23,24]. Among the various dopant ions, strontium is of current interest due to its physicochemical and biological performance in bone repairing process. Sr is also an important element involved in bone metabolism and also promotes preosteoblastic cell proliferation, osteoclast apoptosis and collagen synthesis [25,26]. Sr doped hydroxyapatite, bioactive glass, bone cement have been synthesized [27–31]. Sr doped calcium phosphate coatings have also been investigated [32,33]. Chen et al. reported that strontium phosphate has excellent corrosion resistance compared to manganese phosphate and calcium phosphate coatings [34]. By adding strontium precursor in the phosphating bath, strontium incorporated conversion coatings can be developed. However, there are no literature reports on the effect of dopant ion in the ZCP coating to further improve the bioactivity and corrosion resistance of magnesium alloys. In view of the advantages of both the coating material and coating technique, we have attempted the feasibility of Sr doped ZCP coating by chemical conversion coating method. Hence, the present work deals with the optimization of Sr doped ZCP conversion coating on magnesium AZ31 alloy and its evaluation for bioactivity, corrosion resistance and cytocompatibility.

2. Experimental procedure

2.1. Substrate preparation

AZ31 magnesium alloy was purchased from Exclusive Magnesium, Hyderabad, India. The chemical composition of the alloy is 2.9% Al, 0.88% Zn, 0.001% Fe, 0.02% Mn, and balance magnesium. The alloy was polished with SiC paper up to 1200 grit. The alloy was then washed with double distilled water and ultrasonically cleaned and degreased with acetone.

ZCP and Sr doped ZCP coatings were prepared on the surface of AZ31 alloy in the phosphating bath. The phosphating temperature was maintained at 50° C. The pH of the bath was adjusted to 2.5 with the help of phosphoric acid. The composition of the phosphating bath is 10 g/L diammonium hydrogen phosphate ($(NH_4)_2HPO_4$), 7 g/L zinc nitrate ($Zn(NO_3)_2$), 3 g/L calcium nitrate ($Ca(NO_3)_2$), 3 g/L sodium nitrate ($NaNO_2$), 1 g/L sodium fluoride (NaF). Sr doped ZCP coating was deposited on the substrate by varying the strontium nitrate content (precursor used is strontium nitrate) as 0.5, 1 and 1.5 wt.% with optimized pH of 2.5 at 50° C (optimized temperature) for various deposition times i.e. 5, 10, 15, 20 and 30 min. ZCP coating was also deposited for comparison [35]. Samples were coded as ZCP, 5SZCP, 10SZCP and 15SZCP for undoped, 0.5, 1 and 1.5 wt.% Sr doped ZCP coatings respectively.

2.2. Surface characterization

Fourier transform infrared (FTIR) spectra of ZCP and Sr doped ZCP coatings of various compositions were recorded on an FTIR spectrometer in the range of 400–4000 cm^{-1} with a single reflection ATR accessory (Perkin Elmer Spectrum two, USA). Chemical composition and phases of the compounds were analyzed using X-Ray powder diffractometer (XRD, D8 DISCOVER, Bruker, USA) using Cu k_α radiation at 40 kV and 30 mA at a scan rate of 0.02° Scanning electron microscopy with energy-dispersive X-ray spectroscopy (SEM, FEI, QUANTA 200, NETHERLANDS) was used to characterize the surface morphology and elemental composition of ZCP and Sr doped ZCP coatings. 3D profiles of FESEM images were obtained using scanning probe image processor WSxM 5.0 develop 7.0 software [36]. Contact angle measurements were performed to evaluate the surface wettability of the samples using water with a contact angle instrument (Easy Drop KRUSS, Germany) and a minimum of 10 values were collected per group of samples from different locations.

2.3. Adhesion characterization

Various test methods are available to study the adhesive strength and degradation of the coating. In this work, the adhesion between the coating and the substrate is monitored according to ASTM D 870 [37]. 25 squares were made on the coated substrates using cross cut tester and the coated samples were completely immersed in water in a container which is completely resistant to corrosion. The permeation of water depends on coating characteristics. After 3 days of immersion, the% of the peeled off area of the coating in the squares was evaluated.

2.4. In vitro *degradation and mineralization*

Biomineralisation, weight loss, pH and hydrogen evolution studies were conducted by immersing the samples in simulated body fluid (SBF). Samples with equal dimensions were prepared by coating process as explained in Section 2.1. The procedure for the preparation of SBF was reported by Kokubo and Takadama [38]. Initial pH of SBF was maintained at 37° C for all the experiments. Biomineralisation studies were carried out by immersing the samples in SBF for 15 days to \analyse the deposition of calcium phosphates on the surface.

Immersion test was carried out in SBF for 96 h. The ratio of the surface area of the sample to solution volume was maintained as 1 cm^2: 30 mL [39]. Initial weights of the samples were recorded before immersion in SBF. After

immersion, the samples were cleaned with chromic acid to remove corrosion products. Then, the samples were weighed and corrosion rates were calculated based on Eq. (2)

$$CR = \frac{8.763 \times 10^4 W}{ATD} \quad (2)$$

Where, CR is corrosion rate in mm/yr, W is the weight loss, T is immersion time in h, A is initial surface area in cm^2, D is density of sample ($1.74\,g/cm^2$).

Hydrogen evolution test (HET) was carried out for the period of 96 h to study the evolved hydrogen from corroding sample. The procedure for the HET experiment was in accordance with the earlier report [40,41]. The sample was placed at the center of the beaker containing SBF with a funnel placed over the sample to collect the evolved hydrogen from corroding magnesium. A graduated burette filled with SBF was inverted over the funnel. The evolved hydrogen is collected at the top of the burette by replacing the SBF solution downwards. The initial pH of SBF was maintained as 7.2 and pH were noted down at different time intervals.

The ionic concentrations of the SBF after immersion of the uncoated and coated alloys for known periods were analysed using an Inductive Coupled Plasma-Optical Emission Spectroscopy (Perkin Elmer, Optima 5300 DV, USA) analysis.

2.5. MTT assay

L929 cells (from NCCS, Pune) were cultured with Dulbecco's modified Eagle's medium (DMEM) supplemented with 10% fetal bovine serum, 1% 100 × antibiotic antimycotic liquid and incubated in a CO_2 incubator at 37° C. A cell suspension with DMEM containing 1×10^5 cells were seeded on the sample which was placed in the 9 well cell culture plate and MTT (3-(4,5-Dimethylthiazol-2-Yl)−2,5-Diphenyltetrazolium Bromide) assay was conducted by incubating for 72 h at CO_2 incubator. 200 μL of cell culture medium was added to each well. Then 20 μL MTT solution was added followed with incubation for 4 h at 37 °C. After 4 h incubation, 1 mL of DMSO (Dimethyl Sulphoxide) was added. Viable cells were determined by the absorbance at 540 nm. All the experiments were performed in triplicate.

3. Results

3.1. Surface morphology of the coating

Fig. 1(a–e) shows the surface morphologies of the coatings after immersion in the ZCP phosphating bath for 5, 10, 15, 20 and 30 min respectively. Very few deposits were randomly deposited on the surface during the initial period. With increase in the phosphating time, the size of the deposits became larger and covered the surface. The maximum surface coverage was found at 20 min deposition time. Some cracks were found in the coating due to internal stresses and also the evolution of hydrogen from the dissolving magnesium alloy. As the deposition time was extended up to 30 min, some of the crystal deposits were dissolved in the phosphating bath and the surface was exposed to the medium again (Fig. 1(e) and (j)). Fig. 1(f–j) shows the surface morphology of Sr doped ZCP coated samples. The particles seems to be formed randomly during initial deposition time and the entire surface was covered with the coating with an increase in the deposition time. Although some defective regions were visible in the coating due to the release of hydrogen from the corroding magnesium, the voids were very small suggesting controlled degradation of the alloy. Fig. 2(a–e) shows the cross section of the

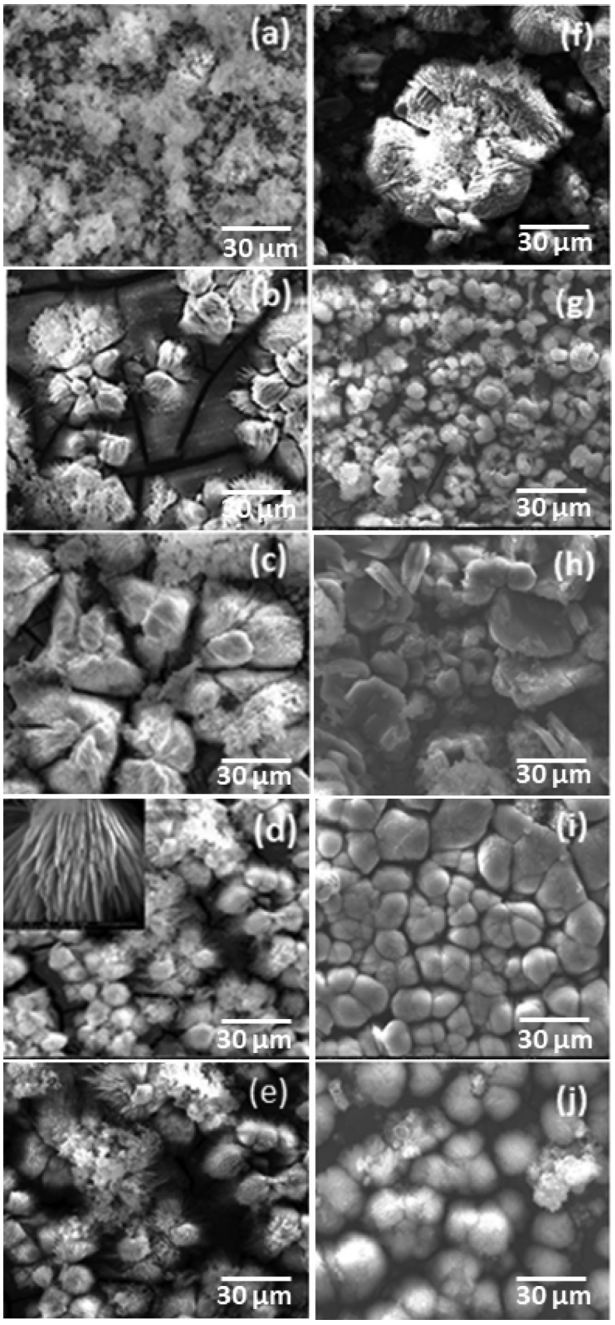

Fig. 1. Surface morphology of ZCP formed at (a) 5, (b) 10, (c) 15, (d) 20 (e) 30 min and Sr doped ZCP coating formed at (f) 5, (g) 10, (h) 15, (i) 20 and (j) 30 min with 0.3 wt.% Sr content.

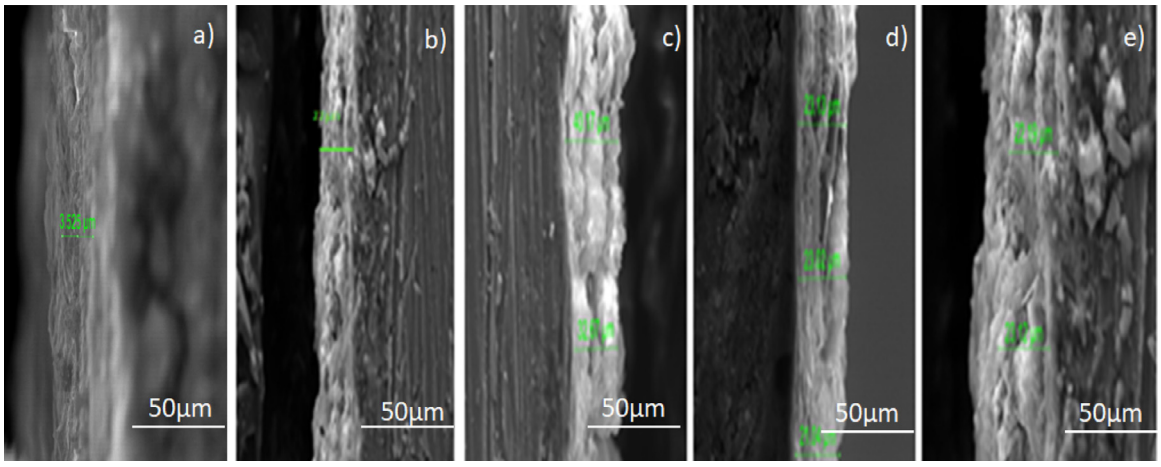

Fig. 2. Cross sections of SEM morphology of ZCP coating formed at (a) 5, (b) 10, (c) 15, (d) 20 and (e) 30 min.

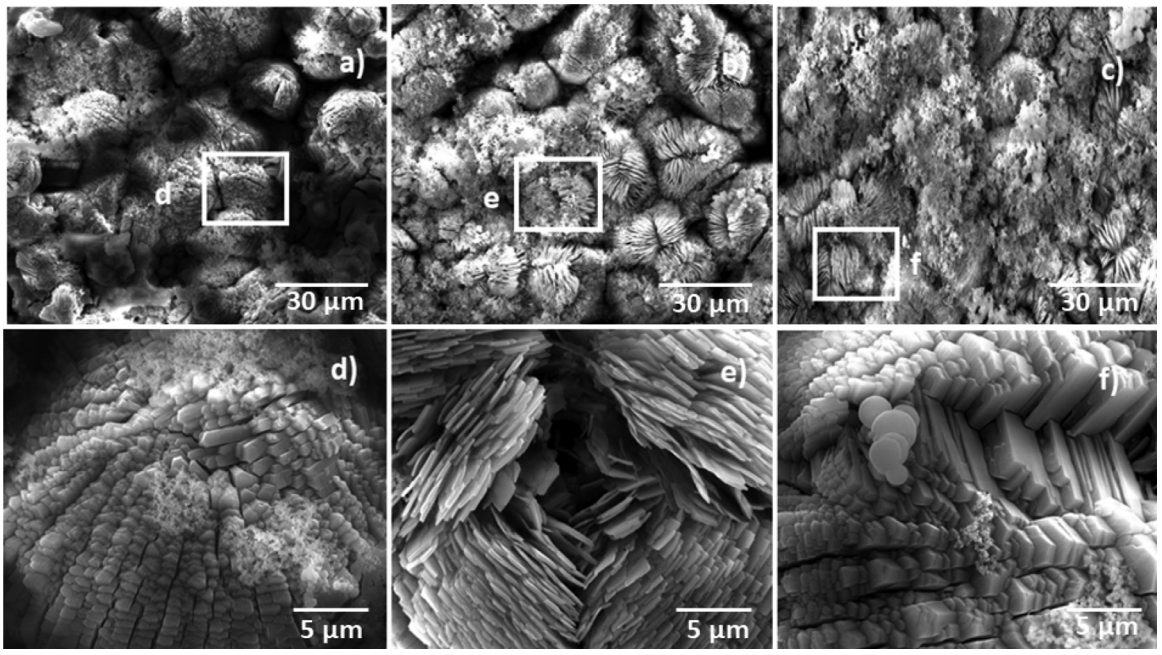

Fig. 3. Surface morphology of Sr doped ZCP coatings formed at 20 min deposition time with (a) 0.5 wt.% Sr (b) 1 wt.% Sr (c) 1.5 wt.% Sr contents.

SEM morphologies of ZCP coating formed at 5, 10, 15, 20 and 30 min. It can be noticed that the thickness of the coating which is formed at 5 min deposition time was 3.525±0.34 µm and 20 min deposition time was 23.13±1.52 µm. Hence, the thickness of the coating has been increased at 20 min deposition time.

As 20 min deposition time is fixed as optimum deposition time, ZCP coating with varying $Sr(NO_3)_2$ content was studied and the morphology of the coatings are shown in Fig. 3 which exhibit slab like particles. Low strontium content in ZCP coating did not cover the entire surface of the alloy. As the strontium content was increased to 1.5 wt.%, the surface was entirely covered with slab like crystals which is oriented in different directions. The coating formed at 50 °C was more compact compared to low phosphating temperature. If coating temperature is further increased, the coating dissolves in the acidic phosphating bath. Hence 20 min deposition time, 50° C temperature and 1.5 wt.% strontium content seems to be optimal parameters for the formation of a crack free coating. Fig. 4 shows the cross sections of surface morphology of Sr doped ZCP coatings formed at 20 min deposition time with 0.5 wt.% Sr, 1 wt.% Sr and 1.5 wt.% Sr contents. The thickness of ZCP coating with 1.5 wt.% Sr content has been greatly improved (46±3.1 µm) compared to low strontium content coatings.

The 3D images of various Sr doped ZCP coatings obtained from SEM images for same configuration are shown in Fig. 5. 5SZCP sample showed more gaps and cracks in the coating, but 15SZCP coated alloy didn't exhibit any cracks. Average roughness value of ZCP coating with 0.5, 1 and 1.5 wt.% Sr substitutions were found to be 58.70, 57.89 and 52.09 µm respectively. Low average roughness (R_a) value of 15SZCP

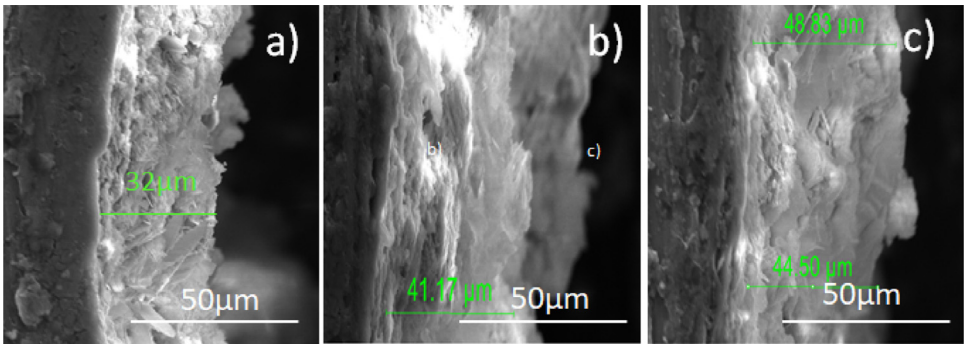

Fig. 4. Cross sections of Surface morphology of Sr doped ZCP coating formed at 20 min deposition time with (a) 0.5 wt.% Sr (b) 1 wt.% Sr (c) 1.5 wt.% Sr contents.

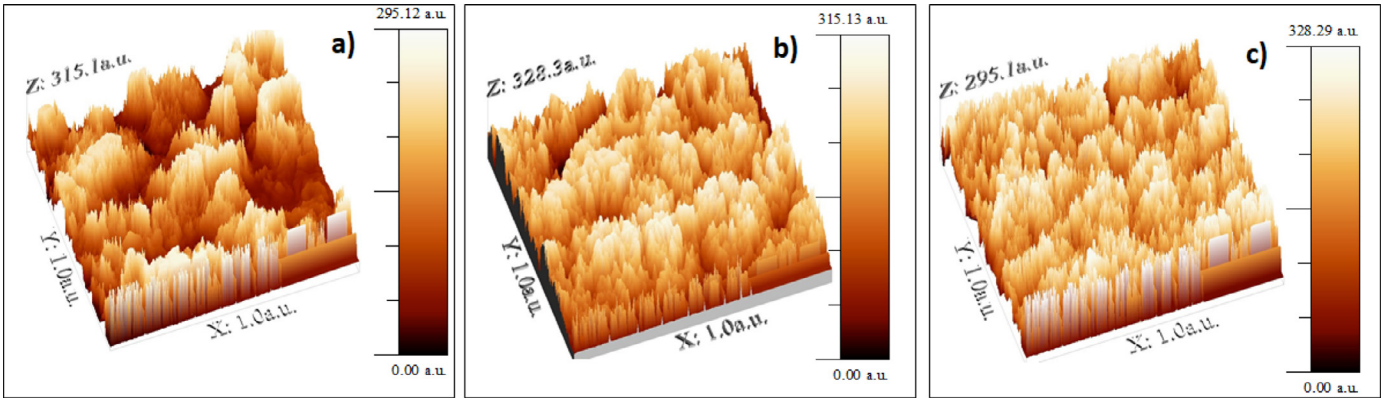

Fig. 5. 3D images of Sr doped ZCP coating formed with (b) 0.5 wt.% Sr (c) 1 wt.% Sr (d) 1.5 wt.% Sr contents (obtained from SEM image).

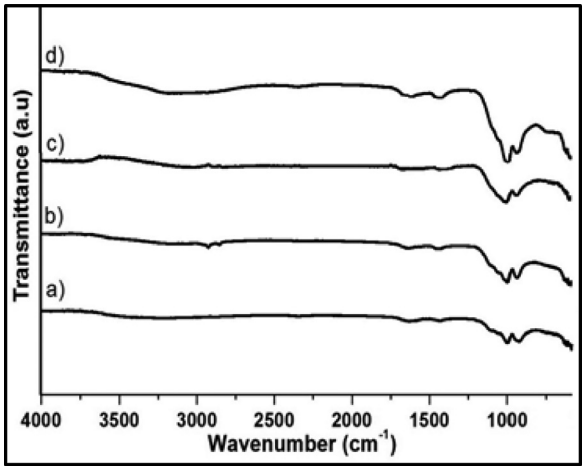

Fig. 6. FTIR spectrum of (a) ZCP and Sr doped ZCP coating formed with (b) 0.5 wt.% Sr (c) 1 wt.% Sr (d) 1.5 wt.% Sr contents.

sample indicated that the surface became more uniform compared to other samples.

3.2. FTIR analysis

FTIR spectra of ZCP and Sr doped ZCP coated samples formed with different strontium nitrate contents are shown in Fig. 6. The phosphate coatings show two strong absorption bands between 900 and 1150 cm^{-1} which is due to the stretching vibration of PO_4^{3-} group. The characteristic bending vibrations of phosphate groups are formed at 550, 610 and 730 cm^{-1} [42].

The broad band around 3250 cm^{-1} and small band around 1680 cm^{-1} correspond to OH^- vibration [43]. Although the spectra look similar to each other, increase in the peak intensity of PO_4^{3-} vibrations around 550 and 1026 cm^{-1} with increasing strontium content in ZCP coating has been observed. The high intense peak of PO_4^{3-} vibrations has appeared for 15SZCP sample. Michele et al. also reported that the intensity of phosphate peak increases with strontium substitution in calcium phosphate coating [44].

3.3. XRD analysis

Fig. 7 shows the XRD patterns of pure and Sr doped ZCP coated samples with various amount of Sr doping. All the XRD pattern closely resemble with each other. The main diffraction peak of (3 2 1) of zinc calcium phosphate (JCPDS 98-000-427), (2 4 1) of zinc phosphate (JCPDS 98-001-8145), (0 2 10) of calcium phosphate (JCPDS 29-359) and (0 4 0) of strontium phosphate phases (JCPDS 96-153-3308) are clearly visible in Figure. It is evident from the XRD analysis that the ZCP coating contains zinc phosphate and zinc calcium phosphate phases. In addition, strontium phosphate phase is also appeared in Sr doped ZCP coated samples [45].

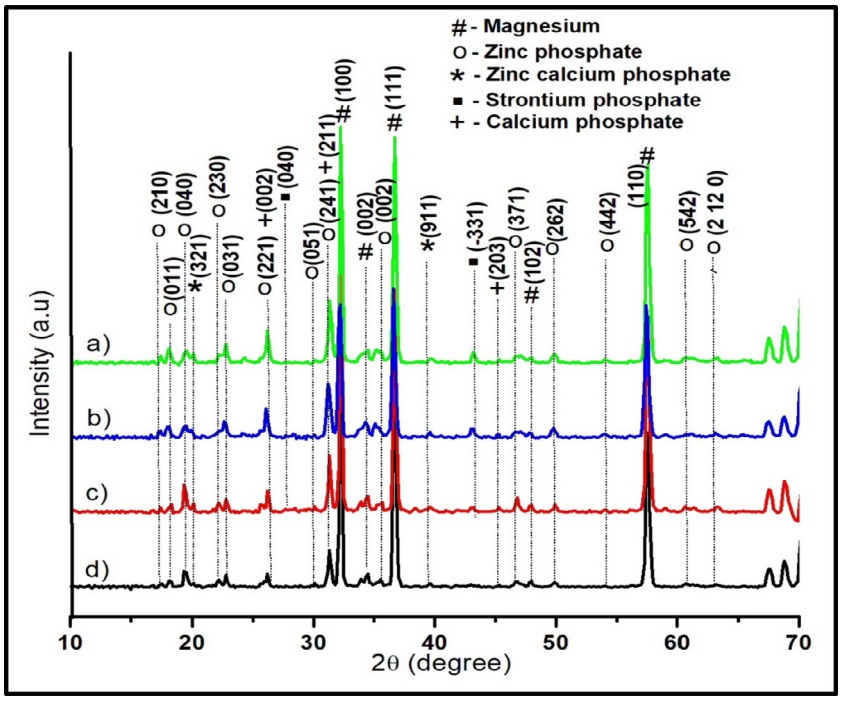

Fig. 7. XRD pattern of (a) ZCP and Sr doped ZCP coating formed with (b) 0.5 wt.% Sr (c) 1wt% Sr (d) 1.5 wt.% Sr contents.

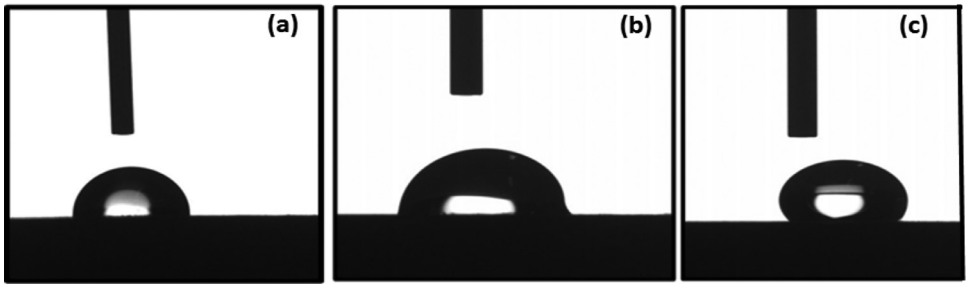

Fig. 8. Contact angle values of AZ31, ZCP and 1.5 wt.% Sr doped ZCP coated AZ31 samples.

3.4. Contact angle measurements

The contact angle values of uncoated, ZCP and Sr doped ZCP coated substrates are shown in Fig. 8. The contact angle of the uncoated alloy is found to be 89±6°, whereas, for ZCP and Sr doped ZCP coatings, the values are 97±11° and 112±18° respectively. High contact angle values suggest that the surface energy of coated surfaces is low, thereby resulting in the hydrophobic behavior of the sample surface.

3.5. In vitro *biomineralization*

The surface morphology of AZ31, ZCP and Sr doped ZCP coated samples after immersion in SBF for 15 days are shown in Fig. 9. The surface of the uncoated AZ31 alloy was severely cracked with less amount of calcium depositions (Fig. 7c). The deposited calcium phosphate was peeled off from the surface due to the continuous corrosion reaction (Fig. 7c). In case of ZCP coating, stable deposits were observed on the surface and size of deposits were found to increase from 38 μm to 43 μm with increase in the immersion time from 10 to 15 days respectively. However, Sr doped ZCP coating exhibits the deposits after five days of immersion and the entire surface was covered with deposits of larger diameter (54 μm) (Fig. 7i) at the final immersion period. The strontium phosphate present in the coating seems to assist in the deposition of more calcium phosphates from SBF [46].

EDX spectra of AZ31, ZCP and Sr doped ZCP coated samples after 15 days of immersion are shown in Fig. 10(a, b, c). All the spectra indicate the presence of Mg, Al, Zn, Ca, and P elements. The Mg, Al, and Zn elements are deposited from the substrate and Ca and P elements are precipitated from SBF. The Ca/P ratio calculated from EDX results for AZ31 was 0.67, while the ratio of ZCP and Sr doped ZCP coating were 1.26 and 1.55 respectively. The higher Ca/P ratio as close to that of hydroxyapatite (Ca/P = 1.67) obtained for Sr doped alloy indicated the improved biomineralization.

Bioactivity of the samples was further characterized using ICP-OES method by monitoring the Mg, Ca and P ions of SBF after immersion of ZCP and Sr doped ZCP coated

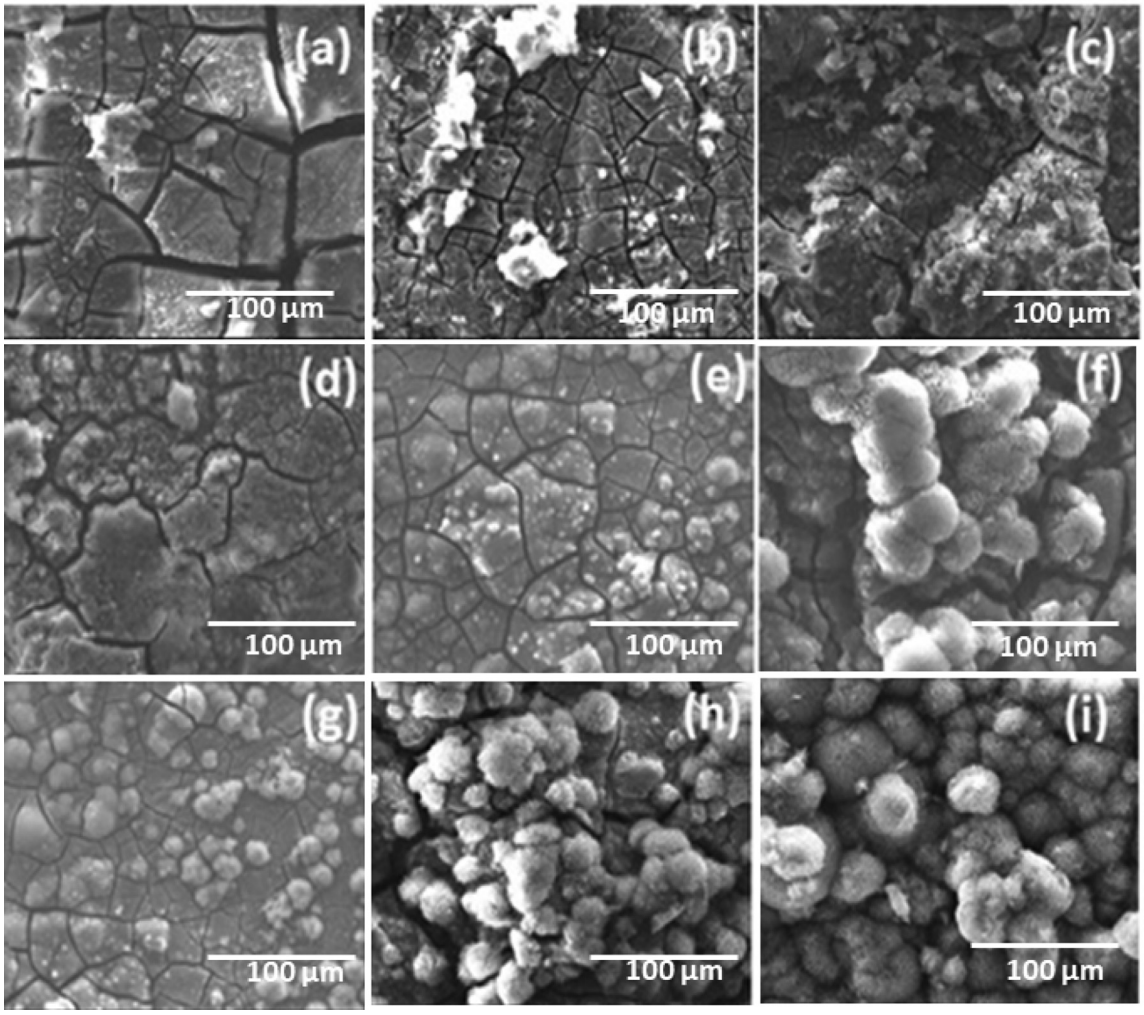

Fig. 9. Surface morphology of AZ31 (a, b and c), ZCP (d, e and f), 1.5 wt.% Sr doped ZCP (g, h and i) coated magnesium alloy after immersion in SBF for 5, 10 and 15 days.

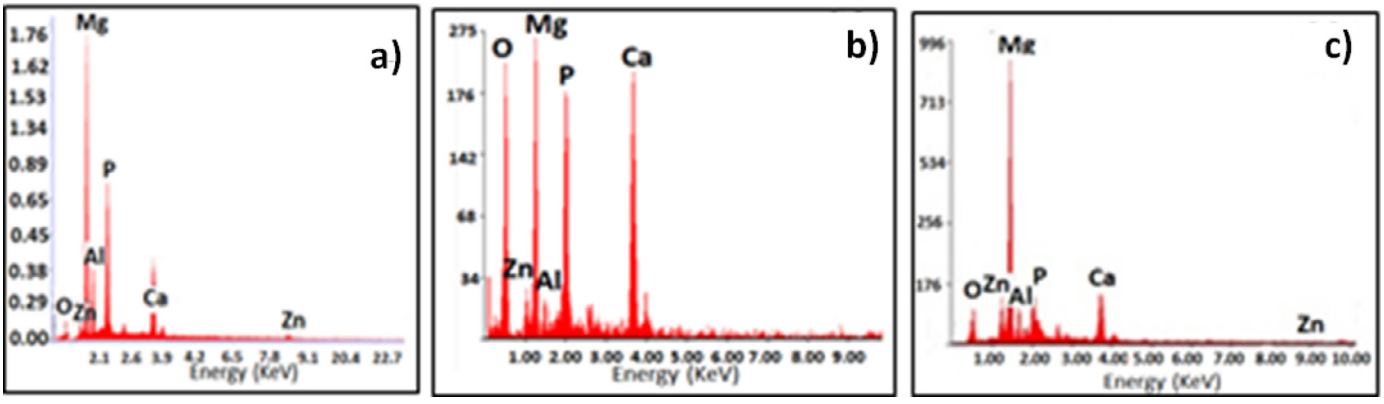

Fig. 10. EDX spectra of AZ31, ZCP and Sr doped ZCP coated samples after 15 days of immersion in SBF.

samples for 96 h. The results as shown in Fig. 11, clearly indicated that the uncoated alloy degraded rapidly and released large amount of magnesium ions into SBF. The Mg ion concentrations of SBF in which the uncoated, ZCP and Sr doped ZCP coated alloys immersed are 160±7.47, 46±3.95 and 23±2.54 mg/L respectively. The amounts of Ca and P ions in SBF of coated alloys were found to be less compared to the uncoated alloy, which may be due to greater amount of mineralization and high affinity of bioactive compounds present on the surface. Remarkably, Ca and P ion concentrations of

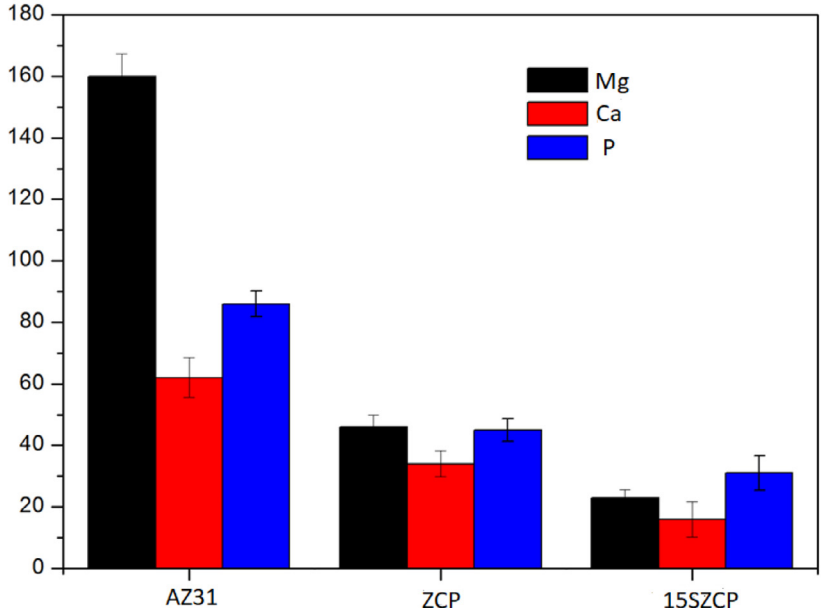

Fig. 11. Mg, Ca, P ion concentrations of SBF after the immersion of AZ31, ZCP and Sr doped ZCP samples for 96 h.

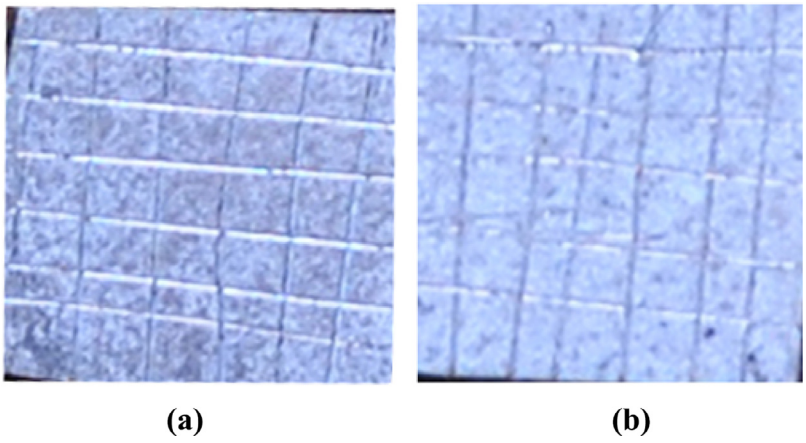

Fig. 12. Photographic images of ZCP and Sr doped ZCP samples.

the SBF which contained 15SZCP sample was very less indicating enhanced bioactivity and leading to slower degradation rate of the substrate.

3.6. Adhesion characterization

Fig. 12(a) and (b) show the photographic images of the ZCP and Sr doped ZCP samples after the test according to ASTM D 870. The delamination of the coatings were evaluated. Eventhough, the coating is present in both the doped and undoped coatings, non-uniform degradation can be observed. The damages are more in ZCP coating than Sr doped coating. The ZCP coating has 60–70% peel off area and the doped coating has only 20–30% peel off area.

3.7. Corrosion charaterisation

3.7.1. Hydrogen gas evolution

The hydrogen evolution results of the uncoated, ZCP and Sr doped ZCP coated samples in SBF are shown in Fig. 13. Hydrogen bubbles come out of the uncoated alloy as soon as it is immersed in the SBF, but the volume of evolved hydrogen decreases after 12 h due to the deposition of calcium phosphates and corrosion products. As the layer undergoes degradation, the hydrogen evolution increases again and the volume of gas collected after the immersion test was 4.35 mL/cm^2/h. In case of ZCP coated samples, the evolved hydrogen was low upto 48 h and the total hydrogen gas collected was 2.25 mL/cm^2/h. In contrast, all the Sr doped conversion coated substrates exhibits low volume of hydrogen

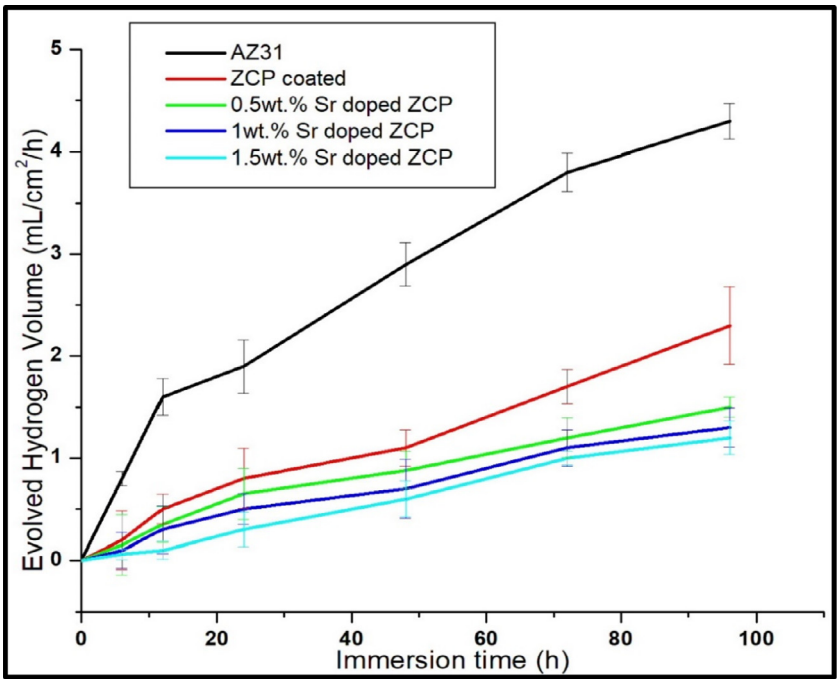

Fig. 13. Hydrogen gas evolution for various samples after 96 h of immersion in SBF.

evolution since the surfaces were much protected compared to uncoated and undoped coated substrates. Particularly, 15SZCP sample has not evolved any bubbles upto 5 h and possessed lowest volume of hydrogen evolution (1.2 mL/cm^2/h) with minimal cracks present in the coating. The 15SZCP sample which contains compact coating delays the ingression of SBF to the alloy surface and avoids fast hydrogen evolution.

3.7.2. pH measurements

The pH variation of SBF containing uncoated and coated samples as a function of immersion time are shown in Fig. 14 and the pH variation follows the same trend of hydrogen gas evolution. The pH of AZ31 immersed SBF increases sharply from 7.2 to 7.7 during the initial immersion time which is due to the release of hydroxide ions into the solution. Subsequently it showed low pH values due to the deposition of corrosion products and calcium phosphate. In contrast, the pH values of SBF of coated samples are lower than that of the uncoated alloy over the entire immersion period. Especially, they exhibited negligible pH raise at the initial immersion time, but showed an increase in pH after initial immersion time which is due to the penetration of solution at the interface between the coating and the substrate via cracks. All the Sr doped samples show low pH change compared to ZCP coated samples. Among Sr doped samples, 15SZCP sample showed the lowest pH variation due to the minimum cracks in the coating. Moreover, the coating exhibits maximum biominaralisation throughout the immersion time.

3.7.3. Corrosion rate

The corrosion rate of the samples with the immersion time in SBF is shown in Fig. 15. The results are in accordance with hydrogen evolution and pH variations. The ZCP coating seems to significantly reduce the corrosion rate of AZ31 from about 2.42 mg/cm^2/h to about 1.35 mg/cm^2/h at the end of immersion. The addition of Sr in ZCP coating further reduces the corrosion rate to 0.67 mg/cm^2/h. It is remarkable that the corrosion rate of 15SZCP sample is one fourth of uncoated AZ31 alloy during the initial immersion time.

3.8. MTT assay

The cell viability of samples was tested with L929 cells using MTT assay and the results are shown in Fig. 16. The coated samples exhibit higher cell viability than uncoated AZ31 alloy. This may be due to the controlled degradation of the alloy. As strontium promotes osteoblast cell proliferation, the 15SZCP sample exhibits the highest cell viability.

4. Discussion

As soon as the samples were immersed in the phosphating solution, the sample surface is divided into two sites, hydrogen evolution and metal matrix dissolution occurring at the micro cathode while the phosphating process initialized by dissolution of magnesium at micro anodic site [47]. Simultaneous evolution of hydrogen from micro cathode results in further increase in local pH at the interface between phosphate solution and alloy surface following with the deposition of insoluble phosphates. The precipitation process preferentially starts with the formation of magnesium phosphate due to the readily available magnesium ions at the surface which is followed by the formation of zinc phosphates and calcium phosphates [48]. Being octahedrally coordinated and identical structure (zinc phosphate and calcium phosphate), zinc and

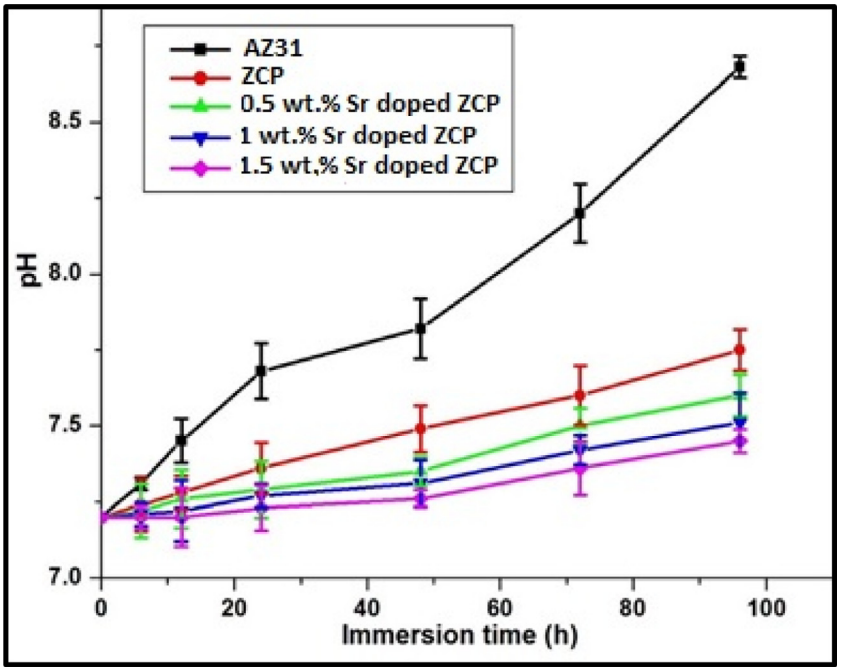

Fig. 14. pH measurements of SBF after immersion of AZ31 and coated samples for 96 h.

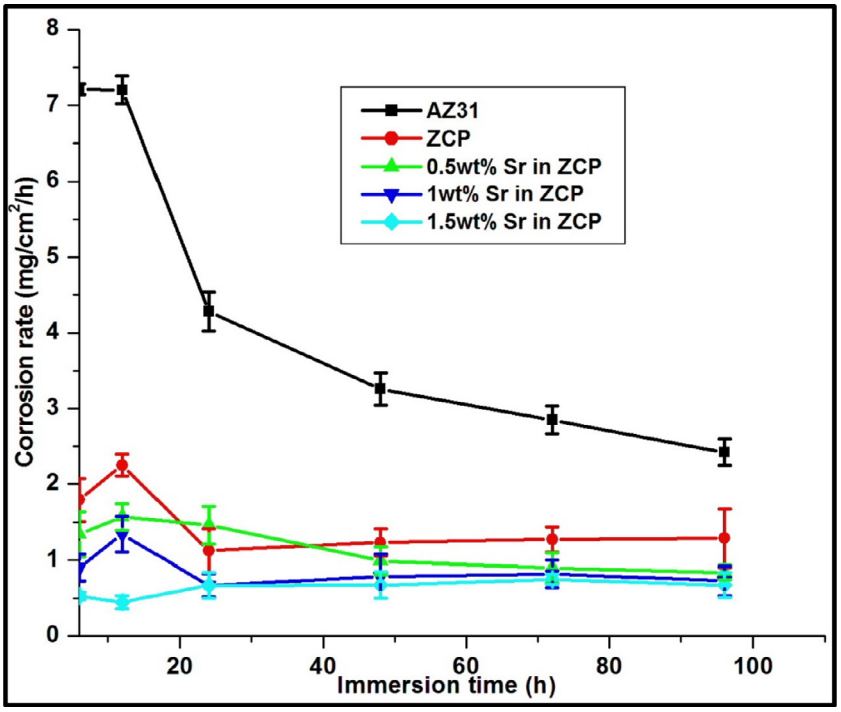

Fig. 15. Corrosion rate of various samples after 96 h of immersion in SBF.

calcium ions exchange with each other resulting in the formation of $CaZn_2(PO_4)_2$. H_2O. In addition, strontium phosphate is precipitated in Sr doped samples during the process. Based on the discussion, a model can be proposed to explain the formation of Sr doped ZCP coating as shown schematically in Fig. 17 involving a) dissolution of magnesium and evolution of hydrogen b) local increase in pH c) precipitation of magnesium phosphate d) formation of alkaline pH surrounding the implant e) precipitation of $Zn_3(PO_4)_2$, $Ca_3(PO_4)_2$, $Zn_2Ca(PO_4)_2$ and $Sr_3(PO_4)_2$ according to the equations

$$H_2PO_4^- \rightarrow HPO_4^{2-} \rightarrow PO_4^{3-} \quad (3)$$

$$3Zn^{2+} + 2PO_4^{3-} + 4H_2O \rightarrow Zn_3(PO_4)_2.4H_2O \quad (4)$$

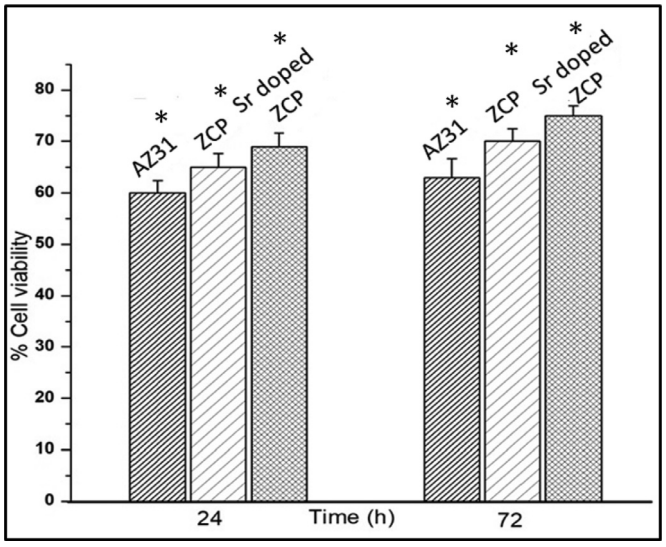

Fig. 16. MTT assay on AZ31, ZCP and Sr doped ZCP coated samples. The significance $P < 0.05$ has been indicated by the asterisk (*).

$$3Zn^{2+} + Ca^{2+} + 2H_2PO_4^- + 4H_2O + 4e^- \rightarrow Zn_2Ca(PO_4)_2.4H_2O + 2H_2O \quad (5)$$

$$3Ca^{2+} + 2PO_4^{3-} + 4H_2O \rightarrow Ca_3(PO_4)_2.4H_2O \quad (6)$$

$$3Sr^{2+} + 2PO_4^{3-} + 4H_2O \rightarrow Sr_3(PO_4)_2.4H_2O \quad (7)$$

The above reactions occur continuously with higher pH conditions until the entire micro anode is covered by crystalline phosphates. The XRD analysis confirms the formation of $Ca_3(PO_4)_2$, $Zn_3(PO_4)_2$ and $Zn_2Ca(PO_4)_2$ phases in undoped coating and additional $Sr_3(PO_4)_2$ formation in doped coatings, but there is no detectable amount of magnesium phosphate phase in the uncoated alloy.

4.1. *Degradation and* in vitro *biomineralization studies*

It is known that magnesium provides only temporary mechanical support and degrades completely after the healing process. One of the important characteristics of bioimplant is that the degradation rate of implant should be matched with the healing rate of bone. Otherwise, the implant will be dissolved and disappeared from the implantation site before the wound heals [49]

The improvement of interface between bone and implant material is an important factor in the development of biomaterials because the formation of viable bone which is close to the surface of the biomaterials are essential for the stability of orthopedic implants. Osseointegration depends on biomineralization which normally happens into the surrounding tissue. Optimum degaradation rate of the implant with faster biomineralization results in osseointegration of bone within the expected time frame. Hence, study on degradation and biomineralization behavior of the uncoated and coated magnesium alloys are essential in the development of novel orthopedic implants.

Adhesion strength, chemical composition, compactness of the coating plays an important role in controlling the degradation of the sample [50]. Since the ZCP conversion coating layer offers immediate protection in SBF, the above reactions are slower than that of uncoated alloy. Prolonged immersion of the coating allows the SBF to reach the surface through gaps and cracks. However, the extension of degradation is less due to stable and adherent compounds such as $Zn_2Ca(PO_4)$, $Zn_3(PO_4)_2$ (from adhesion results) present in the coating and as time passes, it acts as a scaffold for the deposition of calcium phosphates through biomineralization. Hence, biomineralization is much better on ZCP coating. This CaP layer also

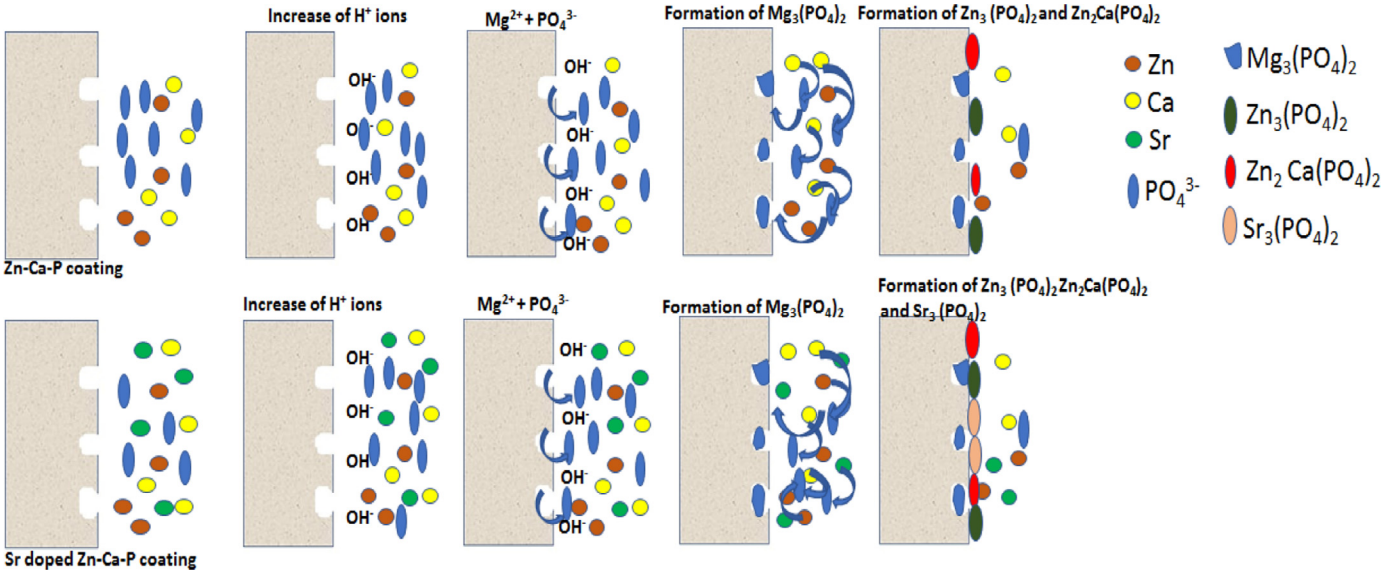

Fig. 17. Schematic diagram representing the mechanism of ZCP and Sr doped ZCP coating.

Table 1
Lists of solubility product of various compounds.

Compounds	Solubility product (K_{sp})
$Mg(OH)_2$	5.6×10^{-12}
$MgCl_2$	3.5×10^{-8}
$Mg_3(PO_4)_2$	1.0×10^{-25}
$Ca_3(PO_4)_2$	2.0×10^{-29}
$Zn_3(PO_4)_2$	9.0×10^{-33}
$Sr_3(PO_4)_2$	1.0×10^{-31}

helps in protecting the surface from degradation and assists in the further deposition of biomineralized products. Hence, Ca/P ratio has been improved at the end of immersion time.

Addition of 0.5 wt.% strontium in ZCP coating enhanced the surface protection of magnesium alloy with better surface coverage of the alloy surface (SEM image Fig. 2(a)). Further the protective efficiency of Sr doping seems to depend on its amount and increase in the Sr doping enhances the compactness of the coating and thereby controlling the degradation rate of the alloy. All the *in vitro* degradation experiments showed that the degradation rate of 15SZCP sample was very much less compared to other doped samples. The reasons are that the surface contains only minimal cracks which resulted in delaying the penetration of the corrosive medium and hydrogen evolution. [51]. Moreover, the solubility product plays an important role in delaying the dissolution of the compounds present in the coating. The stability of the compounds in the coating based on their solubility product value follows the order: $MgCl_2$ < $Mg(OH)_2$ < $Ca_3(PO_4)_2$ <$Zn_2Ca(PO_4)_2$ < $Zn_3(PO_{4)2}$ <$Sr_3(PO_4)_2$ (Table 1). From the order, it is obvious that the presence of strontium phosphate possess low solubility product value and it would strengthen the barrier effect of coating which would further enhance the corrosion resistance.

According to the phenomenon of corrosion mechanism of metallic materials, coating with low contact angle is easily affected by water. Otherwise, the coating with low wettability can effectively prevent the surface from water. Previous literature reports also showed that hydrophobic surface is useful for improving the corrosion resistance of magnesium alloys [52]. In this study, the doped coating has high contact angle value and also possesses highest corrosion resistance. Moreover, it also indicates that the coating contains minimal cracks and pores. From 3D images, it also can be clearly noticed that the coating with higher Sr contains low average roughness value due to uniform surface. Hence, the coated surface resists the ingression of water into the surface, which in turn improves the corrosion resistance. Hence, this hydrophobic, corrosion resistant and uniform surface induces high bioactivity since the deposited calcium phosphate particles during biomineralization do not detatch from the surface. Moreover, the coating also act as a platform for the deposition of calcium phosphates (Ca/P ratio 1.55) from SBF and so the surface is entirely covered with biomineralized products of large size.

In addition, increase in% cell viability at the end of 72 h confirms that ZCP and Sr doped ZCP coatings have not released any toxic ions which could affect the cells involved in osseointegration. In contrast, it helps in controlling the degradation rate of magnesium to control the pH, thereby inducing a favourable environment for cells to grow. Particularly, combination of bioactive strontium phosphate with other corrosion resistant phosphates in the coating improves the cytocompatibility of the alloy by enhancing the surface properties of Sr doped coated samples. Dan Li Fu et al. also indicated that Zn and Sr substituted hydroxyapatite improves cell adhesion and proliferation of osteoblasts and exhibits positive effect on several osteogenic proteins [53]. Hence, the present study shows that controlled degradation and bioactive surface modification of AZ31 by Sr doped ZCP coating can promote cell growth for superior bone healing.

5. Conclusions

Optimal parameters such as pH, temperature, phosphating time and strontium content for the deposition of Sr doped ZCP coating on magnesium alloy using chemical conversion technique has been obtained. Strontium phosphate with low solubility product value has not easily dissolved in the SBF and hence provides more protection in the coating. The 15SZCP sample exhibits low pH, evolved hydrogen volume and corrosion rate. This coating showed improved bioactivity with deposits of Ca/P ratio closer to hydroxyapatite due to the higher induction of calcium and phosphorous by strontium from SBF solution. Hence Sr doped ZCP coated AZ31 alloy may be a suitable degradable implant for orthopedic applications.

Declaration of Competing Interest

The authors declare that they have no known competing financial interests or personal relationships that could have appeared to influence the work reported in this paper.

Acknowledgment

One of the authors, Dr. P. Amaravathy thanks, Department of Science and Technology-Science and Engineering Research Board (DST-SERB), Government of India for providing fellowship under National Post-Doctoral Fellowship (NPDF) scheme.

References

[1] P.R. Cha, H.S. Han, G.F. Yang, Y.C. Kim, K.H. Hong, S.C. Lee, J.Y. Jung, J.P. Ahn, Y.Y. Kim, S.Y. Cho, J.Y. Byun, S.K. Lee, S.J. Yang, H.K. Seok, Sci. Rep. 3 (2013) 2367.
[2] J. Zhuang, Y. Jing, Y. Wang, J. Zhang, H. Xie, J. Yan, J. Orthop. Surg. Res. 11 (2016) 30.
[3] U. Grober, J. Schmidt, K. Kisters, Nutrients 7 (2015) 8199–8226.
[4] R. Swaminathan, Clin. Biochem. Rev. 24 (2003) 47–66.
[5] G.E.J. Poinern, S. Brundavanam, D. Fawcett, D. Fawcett, AJBE 2 (2012) 218–240.
[6] I.B. Singh, M. Singh, S. Das, JMA 3 (2015) 142–148.
[7] A.R. Amini, J.S. Wallace, S.P. Nukavarapu, J. Long Term Eff. Med. Implants 21 (2011) 93–122.

[8] X.N. Gu, Y.F. Zheng, Front. Mater. Sci. 1 (2010) 111–115.
[9] M.S. Uddin, C. Hall, P. Murphy, Sci. Technol. Adv. Mater. 16 (2015) 053501.
[10] N. Nassif, I. Ghayad, Adv. Mater. Sci. Eng. 2013 (2013) 532896.
[11] L.Y. Li, L.Y. Cui, R.C. Zeng, S.Q. Li, X.B. Chen, Y. Zheng, M.B. Kannan, Acta Biomater. 79 (2018) 23–36.
[12] T.S. Sankara Narayanan, Rev. Adv. Mater. Sci. 9 (2005) 130–177.
[13] M.R. Majdi, I. Danaee, S.S.S. Afghahi, Mater. Res. 20 (2017) 445–451.
[14] Y.H. Zou, R.C. Zeng, Q.Z. Wang, L.J. Liu, Q.Q. Xu, C. Wang, ZW. Liu, Front. Mater. Sci. 10 (2016) 281–289.
[15] R. Zeng, Z. Lan, L. Kong, Y. Huang, H. Cui, Surf. Coat. Technol. 205 (11) (2011) 3347–3355.
[16] N. Van Phuong, K. Lee, D. Chang, M. Kim, S. Lee, S. Moon, Met. Mater. Int. 19 (2013).
[17] L.Y. Cui, G.B. Wei, Z.Z. Han, R.C. Zeng, L. Wang, Y.H. Zou, S.Q. Li, D.K. Xu, S.K. Guan, J. Mater. Sci. Technol. 35 (3) (2019) 254–265.
[18] Y. Su, Y. Su, Y. Lu, J. Lian, G. Li, J. Electrochem. Soc. 163 (9) (2016) G138–G143.
[19] R.X. Sun, P.F. Wang, D.D. Zhao, Z.Z. Sun, C.Q. Li, K.Z. Chen, Mater. Corros 66 (2015) 383–386.
[20] S. Horiuchi, M. Hiasa, A. Yasue, K. Sekine, K. Hamada, K. Asaoka, E. Tanaka, J. Mech. Behav. Biomed. Mater. 29 (2014) 151–160.
[21] C.H. Ye, T.F. Xi, Y.F. Zheng, S.Q. Wang, L.I. Yang-de, Trans. Nonferrous Met. Soc. China 23 (2013) 996–1001.
[22] R.C. Zeng, X.X. Sun, Y.W. Song, F. Zhang, S.Q. Li, H.Z. Cui, E.H. Han, Trans. Nonferrous Met. Soc. China 23 (11) (2013) 3293–3299.
[23] H. Chen, E. Zhang, K. Yang, Mater. Sci. Eng. C Mater. Biol. Appl. 1 (2014) 201–206.
[24] R. Radha, D. Sreekanth, J. Magnes. Alloys 5 (3) (2017) 286–312.
[25] C. Liu, H. He (Eds.), Developments and Applications of Calcium Phosphate Bone Cements, Springer Series in Biomaterials Science and Engineering, 2018.
[26] C. Ke, K. Pohl, N. Birbilis, X.-.B. Chen, J. Mater. Sci. Technol. 30 (5) (2014) 5.
[27] C.M. Mardziah, I. Sopyan, M. Hamdi, S. Ramesh, Med. J. Malaysia 63 (2008) 79–80.
[28] V. Nardone, R. Zonefrati, C. Mavilia, C. Romagnoli, S. Ciuffi, S. Fabbri, G. Palmini, G. Galli, A. Tanini, M.L. Brandi, Stem Cells Int. 2015 (2015) 1–12.
[29] J. Isaac, J. Nohra, J. Lao, E. Jallot, J.M. Nedelec, A. Berdal, J.M. Sautier, Eur. Cell. Mater. 21 (2011) 130–143.
[30] R. Jayasree, T.S. Sampath Kumar, R.P. Nankar, Mukesh Doble, Eur. Cell. Mater. 28 (2014) 46.
[31] M. Montesi, S. Panseri, M. Dapporto, A. Tampieri, S. Sprio, PLoS one 12 (2017) e0172100.
[32] S.S. Singh, A. Roy, B.E. Lee, J. Ohodnicki, A. Loghmanian, I. Banerjee, P.N. Kumta, Mater. Sci. Eng. C 40 (2014) 357–365.
[33] T.-D.T. Nguyen, et al., J. Appl. Biomater Function Mater 17 (1) (2019) 2280800019826517.
[34] X.B. Chen, H.Y. Yang, T.B. Abbott, M.A. Easton, N. Birbilis, Surf. Eng. 30 (2014) 871–879.
[35] Rong-chang Zeng, Xin-xin Sun, Ying-wei Song, Fen Zhang, Shuo-qi Li, Hong-zhi Cui, En-hou Han., Trans. Nonferrous Met. Soc. China 23 (11) (2013) 3293–3299.
[36] I. Horcas, R. Fernandez, J.M. Gomez-Rodriguez, J. Colchero, J.W.S.X.M. Gomez-Herrero, A.M. Baro, Rev. Sci. Instrum. 78 (2007) 013705.
[37] Bao-sheng Liu, Ya-fei Kuang, Yue-sheng Chai, Da-qing Fang, Min–gang Zhang, Ying-hui Wei., J. Magnes. Alloys 4 (3) (2016) 220–229.
[38] T. Kokubo, H. Takadama, Biomater 27 (2006) 2907–2915.
[39] H. Huo, Y. Li, F. Wang, Corros. Sci. 46 (2004) 1467–1477.
[40] D. Thirumalaikumarasamy, K. Shanmugam, V. Balasubramanian, J. Magnes. Alloys 2 (2014) 36–49.
[41] A. Stoch, W. Jastrze˛bski, A. Broz˙ek, B. Trybalska, M. Cichocinska, E. Szarawara, J. Mol. Struct. 511–512 (1999) 287–294.
[42] R.L. Frost, R. Scholz, A. López, Y. Xi, Spectrochim. Acta A Mol. Biomol. Spectrosc. 124 (2014) 243–248.
[43] M. Bianchi, L. Degli Esposti, A. Ballardini, F. Liscio, M. Berni, A. Gambardella, S.C. Leeuwenburgh, S. Sprio, A. Tampieri, M. Iafisco, Surf. Coat. Technol. 319 (2017) 191–199.
[44] B. Liu, G.Y. Xiao, Y.P. Lu, J. Electrochem. Soc. 163 (2016) C477–C485.
[45] S. Chen, S. Zhang, X. Ren, S. Xu, L. Yin, Int. J. Electrochem. Sci. 10 (2015) 9073–9088.
[46] R.J. Kavitha, K. Ravichandran, T.S. Narayanan, J. Alloys Compd. 745 (2018) 725–743.
[47] Y. Su, G. Li, J. Lian, Int. J. Electrochem. Sci. 1 (2012) 11497–11511.
[48] R.C. Zeng, F. Zhang, Z.D. Lan, H.Z. Cui, E.H. Han, Corros. Sci. 1 (2014) 452–459.
[49] M. Esmaily, J.E. Svensson, S. Fajardo, N. Birbilis, G.S. Frankel, S. Virtanen, R. Arrabal, S. Thomas, L.G. Johansson, Prog. Mater. Sci. 1 (2017) 92–193.
[50] Y. Xin, K. Huo, H. Tao, G. Tang, P.K. Chu, Acta Biomater 1 (2008) 2008–2015.
[51] D. Song, G. Guo, J. Jiang, L. Zhang, A. Ma, X. Ma, J. Chen, Z. Cheng, Prog. Nat. Sci. Mater. Int. 1 (2016) 590–599.
[52] P. Makkar, H.J. Kang, A.R. Padalhin, I. Park, B.G. Moon, B.T. Lee, PloS One 13 4 (2018) e0193927.
[53] D.L. Fu, Q.H. Jiang, F.M. He, B.P. Fu, J. Zhejiang Univ. Sci. B 1 (2017) 778–788.